Dec. 2015. Vol. 7. No. 05 ISSN2305-8269
International Journal of Engineering and Applied Sciences

www.eaas-journal.org

A REVIEW ON ONE-DIMENSIONAL TWO-PHASE MODEL FOR CRITICAL FLOW BOILING IN MICROCHANNELS

M.Y. ABDOLLAHZADEH JAMALABADI

Assistant Professor Maritime University of Chabahar, Chabahar, 99717-56499, Iran
E-mail: muhammad_yaghoob@yahoo.com

ABSTRACT

Accurate predictions of two-phase pressure drop in a micro diameter passages are necessary for the design of compact and ultra-compact heat exchangers. A semi-experimental model of boiling two-phase pressure drop in the dryout regime is formulated. Prediction of dryout vapor quality is important for design of horizontal flow evaporators. The dryout vapor quality is defined as the local vapor quality at which the two-phase heat transfer coefficient is the maximum. A phenomenological model for predicting dryout vapor quality for annular flow with convective vaporization in plain tubes is proposed, which is comparable with dryout correlations. The model is applicable to high mass flux annular flow in vertical tubes and horizontal tubes for which the effect of stratification due to gravity is negligible.

Keywords: ***Social impact, economic analysis, solid oxide fuel cell, clean energy***

1. INTRODUCTION

Miniaturization of power and refrigeration systems requires the transfer of high heat fluxes at low temperature differences (high heat transfer coefficients) to achieve efficient use of energy. However, although it is generally recognized that heat transfer coefficients can be higher for flow boiling in mini- and micro-channels than in conventional channels, the reduction in cross-section is limited by the increase in pressure drop and the pumping power required to drive the flow. Therefore, accurate prediction of pressure drop is critical for design and optimization of these devices. Many studies have confirmed that the two phase total pressure drop in small and micro tubes increases with decreasing internal tube diameter, Tong et al. [1], Huo et al. [2], Revellin and Thome [3]. A number of studies have reported that there is a clear effect of decreasing tube diameter on flow patterns and their transition boundaries, (Damianides and Westwater [4], Coleman and Garimella [5], Zhao and Bi [6], Chen et al. [7], Kawahara et al. [8] and Revellin and Thome [3]). These include but are not limited to the absence of stratified flow in horizontal channels, diminishing of churn flow and the appearance of additional flow patterns that are not common in normal tubes. These have been mainly attributed to the predominance of surface tension force over gravity. Chen et al. [7] studied the effect of tube diameter on flow pattern transition boundaries for R134a in tubes of 4.26 - 1.1 mm diameter and showed that the slug/churn and churn/annular transition lines shifted towards higher quality as the tube diameter decreased. They also indicated that the slug (periodic) flow regime can exist up to a quality range as high as 0.5 especially at low mass flux values.

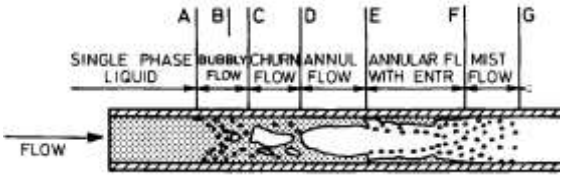

Figure 1. Schematic of the vertical flow boiling process.

These deviations from the conventional understanding raise doubt about the applicability of design methods based on empirical correlations of boiling data in large channels and suggest the necessity for new methods based on flow regimes. Garimella [9] developed a flow regime based model for pressure drop during condensation of refrigerants inside round, square and rectangular passages of hydraulic diameter in the range of 1- 5 mm. Comparison of their model with experiments indicated that flow regime based models yield significantly better pressure drop predictions than traditional empirical correlations, which are

primarily based on air-water mixtures in large diameter tubes. Mechanistic modeling of heat transfer and pressure drop may be more successful for flow boiling in small- to micro- diameter tubes than for large tubes for a number of reasons. For instance, most flow visualization studies report the absence or diminishing of dispersed bubble and churn flows and better - defined liquid/film interfaces as the tube diameter decreases. In addition, flow regimes in small diameter tubes (4.26 -1.1 mm) at low vapour quality (x < 0.3 - 0.5) are dominated by slug flow regime, mostly without trails of small bubbles in the bubble tails. At high quality, annular flow regime is expected. However, beyond a quality of about 0.4 - 0.5 transient dryout is deduced from the heat transfer measurements in many studies.

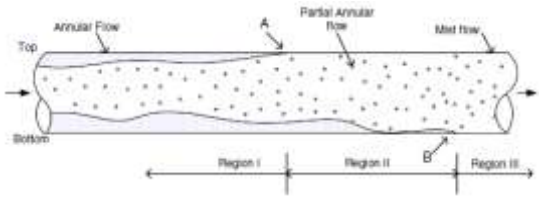

Figure 2. Shear stress distribution in horizontal annular flow.

Therefore, a model based on the periodic flow of bubble slugs is likely to be a reasonable approach to the prediction of heat transfer and pressure drop. The one-dimensional model for pressure drop in slug flow presented here follows the approach of the three-zone evaporation model developed by Thome et al. [10] for predicting flow boiling heat transfer. The results are compared with experimental data collected using R134a for five stainless steel tubes of internal diameter 4.26, 2.08, 2.01, 1.1 and 0.52 mm. Other parameters were varied in the ranges mass flux 100 – 500 kg/m^{2}s, pressure 6 – 12 bar, quality up to 0.9, heat flux 13 - 150 kW/m^2.

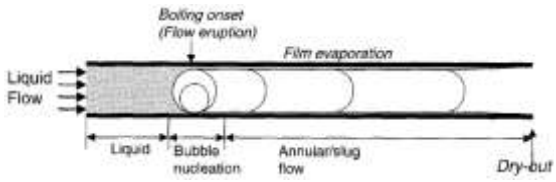

Figure 3. Surface tension is dominant and gravity is negligible in micro-channels

2. FLUID FLOW MODEL

The assumptions in the Thome et al. [10] model are given in detail here because they are the basis for the subsequent pressure drop model:

1. Confined-bubble flow, sequence: liquid, vapour + evaporating film, vapour only.
2. Fluctuation period t_b set by the nucleation period at a single upstream site.

This period is not determined by experimental observation but by modifying a correlation based on pool boiling to optimise the fit of the complete heat transfer model to a large data base for heat transfer coefficients for a range of fluids and conditions:

$$t_b = \left(\frac{3328}{q}\right)^{1.74}\left(\frac{p_{crit}}{p}\right)^{0.87} \quad (1)$$

The dimensional nature of this correlation indicates that further development of the model is required.
Negligible film thickness δ compared to channel cross-section dimensions, $\delta << D.$
Negligible transport of liquid by motion of the film (following from 3).
Negligible effect on flow area for vapour (also following from 3).

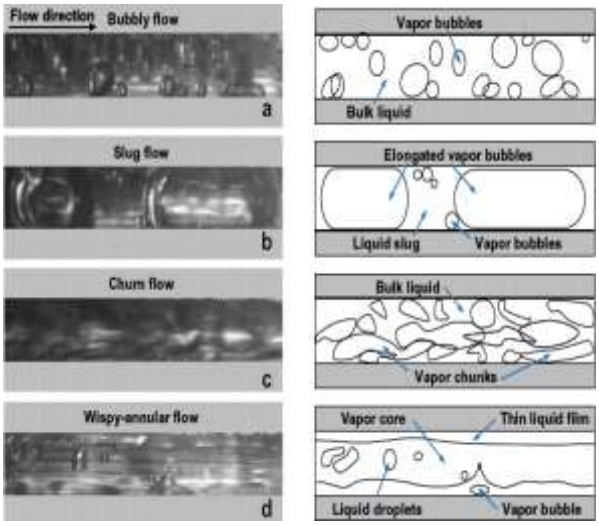

Figure 4. Flow boiling regimes in micro-channels

Homogeneous flow. A liquid slug and the head of the bubble immediately behind it have the same velocity, the "pair velocity" Up, given by

$$U_p = G\left[\frac{x}{\rho_v} + \frac{1-x}{\rho_l}\right] \quad (2)$$

and the residence times of alternating liquid t_l and vapour (with and without liquid film) t_v during a cycle of period tb are given by

$$\frac{t_l}{t_b} = \frac{1}{1+\frac{\rho_l}{\rho_v}\frac{x}{1-x}} \quad , \quad \frac{t_v}{t_b} = \frac{1}{1+\frac{\rho_v}{\rho_l}\frac{1-x}{x}} \quad (3)$$

where x(z) is the local time-averaged mass fraction of vapour at axial distance z.

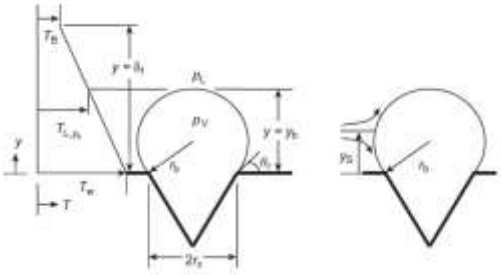

Figure 5. Heat transfer mechanisms of boiling in micro-channels

7.Thermal equilibrium between phases, so that x may be calculated from a time-averaged enthalpy balance for a specified heat input per length of channel with all phases at the local saturation temperature.

8.The initial liquid film thickness of formation δ0 (z) is calculated from an empirical correlation δ0/D = F(Bo) given by Moriyama and Inoue [11], corrected by a factor equal to 0.29 by Dupont et al. [12]:

$$\frac{\delta_0}{D} = 0.29\left(\frac{\nu_l}{U_p D}\right)^{0.28}\left[\left(0.07Bo^{0.41}\right)^{-8} + 0.1^{-8}\right]^{-1/8} \quad (4)$$

where the Bond number Bo is defined by

$$Bo = \rho_l D U_p^2 / \sigma \quad (5)$$

This is the only feature of the model that involves surface tension σ , which is generally assumed to be the dominant influence on the progression from small to mini- to micro-channels.

9. After formation, the film is assumed to be stationary relative to the wall. Its thickness δ (t) decreases by evaporation and therefore depends on the model for heat transfer. The Thome et al. [10] model assumes constant, uniform heat flux *q* from the wall to whatever fluid is in contact with it (liquid, liquid film, vapour). For liquid and vapour, the bulk temperature is assumed to be T_{sat} *(p)*, where *p* is the time-averaged pressure, and heat transfer coefficients are obtained from conventional correlations for fully-developed flow with U_p *(z)* as the bulk velocity, despite the possibly short lengths of slugs and bubbles and consequent internal circulation patterns. The assumptions for heat transfer through the film are steady conduction with the liquid-vapour interface at T_{sat} *(p)*. The film thickness at time *t* after formation is then

$$\delta = \delta_0 - qt/\rho_l h_{lv} \quad (6)$$

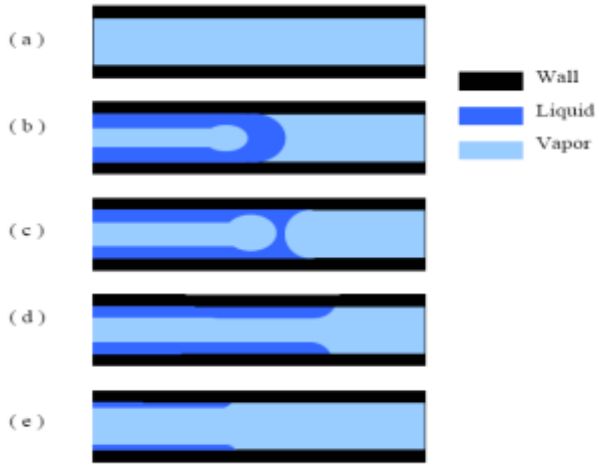

Figure 6. Annular to CHF in Schematic Form. (a) channel dry-out, (b) annular slug with liquid head, (c)contact angle shift, (d) vapor penetration at CHF occurrence, (e) thinning film as it returns to dry-out

The film is assumed to break up at a minimum thickness δ min, the value being chosen to optimise the fit of the entire heat transfer model to a database. A more physically based choice may be of the order of the wall roughness, Thome et al. [10], Shiferaw et al. [13]. The evaporation time te is given by

$$t_e = \left(\delta_0 - \delta_{\min}\right)\rho_l h_{lv} / q \quad (7)$$

If $t_e < t_v$, there is a period of vapour-only flow equal to $t_e - t_v$.

If $t_e > t_v$, the film evaporates to a thickness at the end of the bubble given by

$$\delta_{end} = \delta_0 - qt_v / \rho_l h_{lv} \quad (8)$$

It is assumed that survival of the film has no influence on conditions in the following liquid slug. The equations for change in film thickness would be modified if a different heat transfer model were used, e.g. transient conduction in a film on a wall of finite thickness.

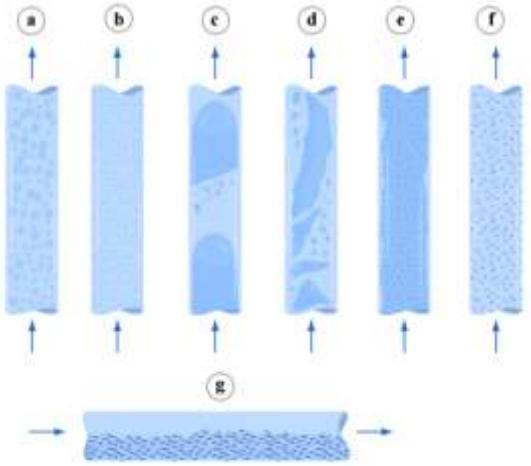

Figure 7. Typical configuration of (a) bubbly flow, (b) dispersed bubbly (i.e. fine bubbles dispersed in the continuous liquid phase), (c) plug/slug flow, (d) churn flow, (e) annular flow, (f) mist flow (i.e. fine droplets dispersed in the continuous vapor phase) and (g) stratified flow. Note: mist flow is possible only in a heated channel; stratified flow is possible only in a horizontal channel.

3. HEAT TRANSFER MODEL

The assumption of homogeneous time-averaged flow is central to the Thome et al. [10] heat transfer model, leading to a relatively straightforward approach to predicting time-averaged wall temperature for a constant wall heat flux without the need to track the development of individual bubbles. Consequently local fluctuations in pressure or velocity are not modelled and only the time-averaged homogeneous velocity Up (z) can be used for the bulk phase velocities and other inputs to the local mechanistic models such as liquid film thickness.

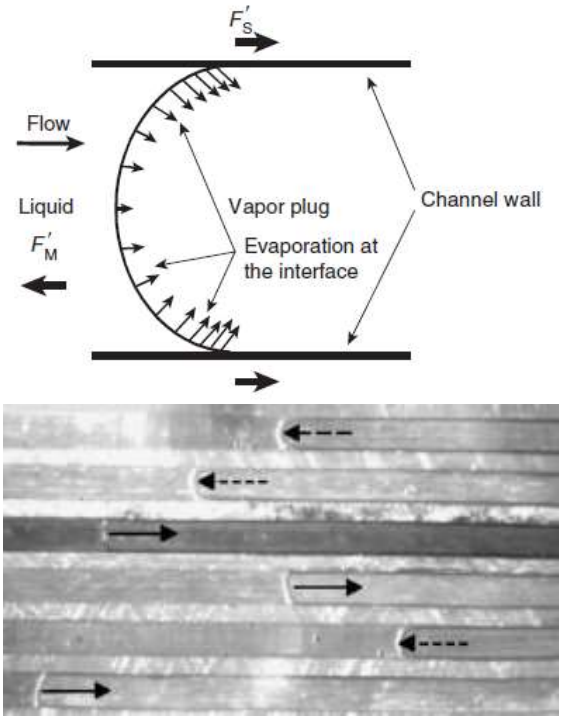

Figure 8. Schematic representation of evaporation momentum and surface tension forces on an evaporating interface in a microchannel.

During the time fractions corresponding to single phase liquid or vapour flow, the heat transfer coefficients αl ,αv are calculated from correlations for fully developed flow using Up (z) and the relevant single phase properties. In film flow, the heat transfer coefficient is estimated for conduction through the mean film thickness δm :

$$\alpha_f = 2k_l / (\delta_0 + \delta_{\min}) \quad \text{or} \quad \alpha_f = 2k_l / (\delta_0 + \delta_{end}) \tag{9}$$

Time-averaging wall temperature with constant wall heat flux is equivalent to calculating the time-averaged heat transfer coefficient α (z) from

$$\frac{1}{\alpha} = \frac{1}{\alpha_l}\frac{t_l}{t_b} + \frac{1}{\alpha_f}\frac{t_e}{t_b} + \frac{1}{\alpha_v}\frac{(t_v - t_e)}{t_b} \tag{10}$$

This mechanistic method replaces in the homogeneous model the calculation of α from a single-phase convective correlation of the form Nu = f (Re, Pr), using expressions for homogeneous properties such as

$$c_h = xc_v + (1-x)c_l \tag{11}$$

$$\frac{1}{k_h}=\frac{x}{k_v}+\frac{(1-x)}{k_l} \quad (12)$$

$$\frac{1}{\rho_h}=\frac{x}{\rho_v}+\frac{(1-x)}{\rho_l} \quad (13)$$

$$\frac{1}{\mu_h}=\frac{x}{\mu_v}+\frac{(1-x)}{\mu_l} \quad \text{or}$$

$$\mu_h = x\mu_v = (1-x)\mu_l \quad (14)$$

For liquid and vapour slugs of finite length, the homogeneous flow assumption is an approximation and the assumption of local thermal equilibrium between phases leads to inconsistencies. There can be no superheating of the liquid or vapour so the enthalpy of the thin film must be negligible and all the heat transferred to the liquid and vapour phases in the absence of a thin film must somehow be transferred by internal mixing to a liquid-vapour interface to cause evaporation.

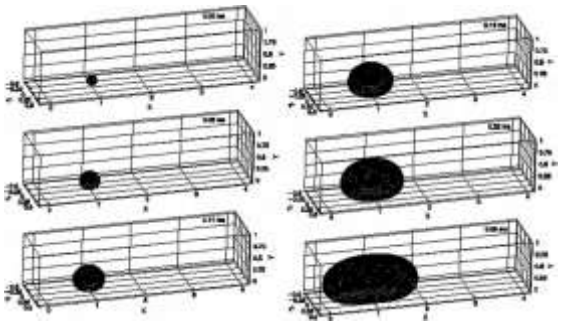

Figure 9. Simulation of bubble growth in a microchannel, with upstream to downstream flow

The local heat transfer coefficient is calculated as a sum of the two contributions i.e., nucleate and convective. Various correlations have been proposed by different people for calculating the local heat transfer coefficient but the correlation proposed by Kandlikar[1] in 2004 has relatively good agreement with experimental data for a broad range of spectrum of fluids over a wide range of conditions. Eqn [ ] gives expression for calculating local heat transfer coefficient as proposed by Kandlikar [1]. In the equation, Fr_{Lo} represents the Froude number with all flow as liquid. Since the effect of Froude number is expected to be small in microchannels, the function $f_2(Fr_{LO})$ is taken as 1.0.

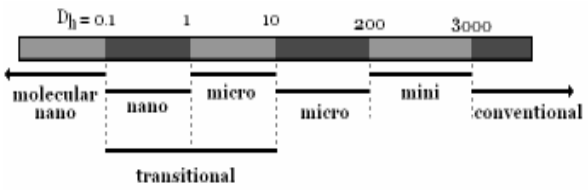

Figure 10. channel classification

The single-phase, all-liquid flow heat transfer coefficient h_{LO} is given by appropriate correlations depending on the Reynolds number of the turbulent flow. For microchannels with the all-liquid flow in the laminar region, h_{LO} is evaluated using the fact that Nusselt number is constant where the constant depends on the channel geometry and the wall thermal boundary condition. *Co*, *Bo* in the equation represent Convection number and Boiling number respectively and their expressions are given in Eqn [1] and [2].

$$h_{TP} = \text{larger of}\begin{Bmatrix} h_{TP,NBD} \\ h_{TP,CBD} \end{Bmatrix}$$

$$h_{TP,NBD} = 0.6683Co^{-0.2}(1-x)^{0.8} f_2(Fr_{LO}) h_{LO}$$
$$+1058.0Bo^{0.7}(1-x)^{0.8} f_2(F_{FL}) h_{LO}$$

$$h_{TP,CBD} = 1.136Co^{-0.2}(1-x)^{0.8} f_2(Fr_{LO}) h_{LO}$$
$$+667.2Bo^{0.7}(1-x)^{0.8} f_2(F_{FL}) h_{LO}$$

$$Co = \left[(1-x)/x\right]^{0.8}(\rho_v/\rho_l)^{0.5},$$

$$Bo = q''/Gh_{LV}$$

The use of turbulent flow correlations was found to be appropriate for Re_{LO} >3000, while for Re_{LO} <1600, the use of laminar flow correlation yielded good agreement. In the transition region, a linear interpolation was recommended between the limiting Re_{LO} values of 1600 and 3000. With further reduction in the Reynolds number, Re_{LO} <300, it was found that the flow boiling mechanism is nucleate boiling dominant and the use of only the nucleate boiling dominant expression in Eqn [5] for $h_{TP,NBD}$ is appropriate in the entire range of vapor quality. Thus the following scheme given in Eqn [5] is recommended for Re_{LO} <300.

$$h_{TP} = h_{TP,NBD} \; for \; \mathrm{Re}_{LO} < 300$$

4. TWO-PHASE PRESSURE DROP MODEL

Nondimensional number , their significance and relevance to microchannels are :

Martinelli parameter, Ratio of frictional pressure drops with liquid and gas flow; Co , a modified Martinelli parameter, used in correlating flow boiling heat transfer data Its direct usage beyond flow boiling correlations may be limited Boiling number, Bo , Heat flux is nondimensionalized with mass flux and latent heat, K1 , the ratio of evaporation momentum to inertia forces at the liquid-vapor interface is applicable to flow boiling systems where surface tension forces are important ;K2 , the ratio of evaporation momentum to surface tension forces at the liquid-vapor interface is applicable in modeling interface motion, such as in critical heat fluxl Bond number, the ratio of buoyancy force to surface tension force; used in droplet and spray applications (Since the effect of gravitational force is expected to be small, Bo is not expected to play an important role in microchannels); Eotvos number, similar to Bond number; Capillary number, , the ratio of viscous to surface tension forces (useful in bubble removal analysis); Ohnesorge number, the ratio of viscous to the square root of inertia and surface tension forces (used in atomization), Weber number, the ratio of the inertia to the surface tension forces; Jakob number, the ratio of the sensible heat required for reaching a saturation temperature to the latent heat.

$$\frac{\partial}{\partial t}(\alpha_v \rho_v \boldsymbol{V}_v) + \boldsymbol{\nabla}.(\alpha_v \rho_v \boldsymbol{V}_v \boldsymbol{V}_v) = -\boldsymbol{\nabla}.(\alpha_v P) + \boldsymbol{\nabla}.(\boldsymbol{\mu'}_{eff,v}(\boldsymbol{\nabla} V_v + \boldsymbol{\nabla} \boldsymbol{V}_v^T)) + \boldsymbol{F}_{d,v} + \Gamma_{lv} V_l + \alpha_v \rho_v \mathrm{g}$$

$$\frac{\partial}{\partial t}(\alpha_l \rho_l \boldsymbol{V}_l) + \boldsymbol{\nabla}.(\alpha_l \rho_l \boldsymbol{V}_l \boldsymbol{V}_l) = -\boldsymbol{\nabla}.(\alpha_l P) + \boldsymbol{\nabla}.(\boldsymbol{\mu'}_{eff,l}(\boldsymbol{\nabla} V_l + \boldsymbol{\nabla} \boldsymbol{V}_l^T)) + \boldsymbol{F}_{d,l} + \Gamma_{vl} V_v + \alpha_l \rho_l \mathrm{g}$$

$$\boldsymbol{\mu'}_{eff} = \alpha_i \mu_i F_d = \frac{1}{8\rho_l A_{lv} c_d |V_l - V_v|(V_l - V_v)}$$

$$c_d = \frac{24}{Re}(1 + 0.1 Re_b^{0.75}), \quad Re \le 500$$

$$Re_b = \frac{\rho_l |V_l - V_v| d_b}{\mu_l}$$

Applying this approach to the prediction of pressure drop, a direct consequence of the homogeneous flow and local thermal equilibrium assumptions is that the time averaged gravitational and acceleration contributions to the pressure gradient may be calculated from the axial distribution of heat input and Eq. (13). For uniform heat flux, vertical upward flow in a circular tube

$$x = \frac{4q}{Gh_{lv}} \frac{z}{D},$$

$$\frac{dp_{grav}}{dz} = -\rho_h g = -\frac{\rho_l g}{\left(1 + \frac{4qv_{lv}}{DGh_{lv}v_l} z\right)},$$

$$\frac{dp_{acc}}{dz} = -G\frac{dU_p}{dz} = -\frac{4Gqv_{lv}}{Dh_{lv}} \quad (15)$$

The time-averaged wall shear stress and frictional pressure gradient are calculated by time-sharing between estimates for the liquid-only, vapour + liquid film and vapour-only regimes:

$$\tau_w = \tau_l \frac{t_l}{t_b} + \tau_f \frac{t_e}{t_b} + \tau_v \frac{(t_v - t_e)}{t_b},$$

$$\frac{dp_{fric}}{dz} = -\frac{4\tau_w}{D} \quad (16)$$

The total time-averaged pressure gradient is the sum of the three time-averaged contributions:

$$\frac{dp}{dz} = \frac{dp_{grav}}{dz} + \frac{dp_{acc}}{dz} + \frac{dp_{fric}}{dz} \quad (17)$$

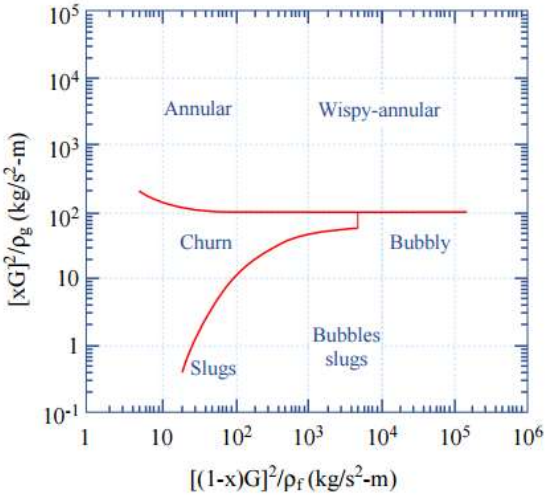

Figure 11. A typical flow map obtained from data for low-pressure air-water mixtures and high-pressure water-steam mixtures in small (1-3 cm ID) adiabatic tubes

For the single-phase regimes, the Thome et al. [10] approach of using correlations for heat transfer in fully-developed flow based on the local homogeneous velocity U_P is applied to the estimation of the friction coefficients, with the same reservations noted in the previous section. In the examples given later in this paper, the Reynolds

number calculated from the homogeneous velocity and the single phase properties is always greater than 2000 except for the 0.52 mm diameter tube.
For this tube, Reynolds number based on single phase vapour properties is less than 2000 especially at low vapour qualities. So standard correlations such as the Blasius equation for fully-developed turbulent and *16/Re* for laminar flow are used:

$$\tau_i = \begin{cases} \dfrac{0.0791}{\mathrm{Re}^{1/4}} \dfrac{\rho U_p^2}{2} & \text{turbulent} \\ \dfrac{16}{\mathrm{Re}} \dfrac{\rho U_p^2}{2} & \text{laminar} \end{cases} ,$$

$$\mathrm{Re} = \frac{\rho U_p D}{\mu} \qquad (18)$$

where ρ, μ are for liquid-only or vapour-only.
The presence of a thin evaporating liquid film during interval t_e may have three hydrodynamic consequences.

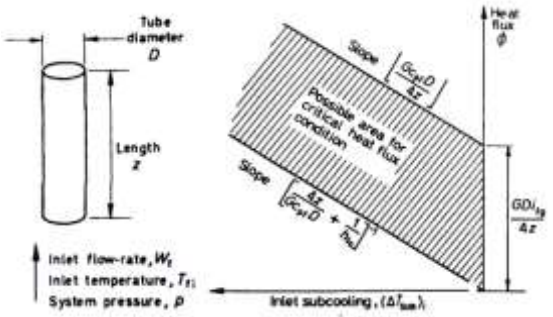

Figure 12. Independent variables affecting the critical heat flux for uniformly heated vertical round ducts and the limits of the critical heat flux condition.

(i) The flow area for the vapour flow is reduced. In the simple approach presented here, this effect is neglected, consistent with assumptions 3 and 4 in the Thome model that $\delta << D$. (There may be circumstances in which this condition is not valid, which should be checked with Eq. (4)). The bulk velocity in the vapour is then equal to the velocity of the vapour without a film, assumed to be U_p.

$$\frac{\partial}{\partial t}(\alpha_v \rho_v) + \boldsymbol{\nabla}.(\alpha_v \rho_v \boldsymbol{V}_v) = \boldsymbol{\nabla}.(\rho_v \boldsymbol{D}_v \boldsymbol{\nabla}\alpha_v) + \Gamma_{lv}$$

$$\frac{\partial}{\partial t}(\alpha_l \rho_l) + \boldsymbol{\nabla}.(\alpha_l \rho_l \boldsymbol{V}_l) = \boldsymbol{\nabla}.(\rho_l \boldsymbol{D}_l \boldsymbol{\nabla}\alpha_l) + \Gamma_{vl}$$

(ii) Instabilities at the liquid-vapour interface may increase its effective roughness, an effect that is known to be important in large channels. For now, it is assumed that the interface remains smooth.

$$\Gamma_{lv} = \frac{h_{lv} A_{lv} (T_{sat} - T_l)}{h_{fg}}$$

$$\Gamma_{vl} = \frac{h_{lv} A_{lv} (T_l - T_{sat})}{h_{fg}}$$

$$h_{lv} = \frac{N_u k_l}{d_b}$$

$$N_u = 2 + 0.6 (Re_b)^{0.5} \mathrm{pr}^{0.3}$$

$$A_{lv} = \frac{6\alpha_v}{d_b}$$

$$d_b = 0.5\, d_{max}$$

$$d_{max} = \frac{\sigma We_{crit}}{\rho_l (V_l - V_g)^2}$$

(iii) Motion of the liquid film with an interfacial velocity of U_i reduces the velocity for calculation of the interfacial shear stress τ_i exerted by the vapour to $(U_p - u_i)$. Eq.(18) becomes

$$\tau_i = \begin{cases} \dfrac{0.0791}{\mathrm{Re}^{1/4}} \dfrac{\rho_v (U_p - u_i)^2}{2} & \text{turbulent} \\ \dfrac{16}{\mathrm{Re}} \dfrac{\rho_v (U_p - u_i)^2}{2} & \text{laminar} \end{cases}$$

$$\mathrm{Re} = \frac{\rho_v (U_p - u_i) D}{\mu_v} \qquad (19)$$

,
This effect is estimated by an approximate model that does not attempt to follow the nonlinear reduction in film thickness with time. Instead, quasi-steady, parallel flow is assumed in a film of constant and uniform thickness δ_m equal to the average of the initial thickness δ_0 and the final thickness δ_{min} or δ_{end}, as calculated by the methods in the heat transfer model.
In a vertical tube, the film is subjected to the same total pressure gradient *dp/dz* as the adjacent gas phase, a gravitational body force $\rho_l g$, a wall shear stress τ_f and an interfacial shear stress τ_i , Fig. 1. Consistent with the steady-flow approximation, the changes in momentum of the film are assumed negligible. For a planar approximation consistent

with $\delta_m << 1$, the velocity distribution for laminar flow in the film is given by

$$u = \frac{\tau_i}{\mu_l} y + \left[\frac{dp}{dz} + \rho_l g\right] \frac{y}{\mu_l}\left(\frac{y}{2} - \delta_m\right) \quad (20)$$

$$u_i = \frac{\tau_i}{\mu_l}\delta_m - \left[\frac{dp}{dz} + \rho_l g\right] \frac{\delta_m^2}{2\mu_l} \quad (21)$$

and

$$\tau_f = \tau_i - \left[\frac{dp}{dz} + \rho_l g\right]\delta_m \quad (22)$$

The pressure gradient in the vapour during the thin-film period is not equal to the time-averaged pressure gradient and is given by

$$\frac{dp}{dz} = \frac{dp_{grav}}{dz} + \frac{dp_{acc}}{dz} + \frac{dp_{fric}}{dz} = -\rho_v\left[g + U_p \frac{dU_p}{dz}\right] - \frac{4\tau_i}{D}\left(1 - \frac{\delta_m}{D}\right)$$

$$\approx -\rho_V\left[g + U_p \frac{dU_p}{dz}\right] - \frac{4\tau_i}{D} \quad (23)$$

The wall shear stress τ_f *(z)* is obtained by simultaneous solution of Eqs. (19, 21-23) with inputs $U_p(z)$, $dU_p/dz(z)$ and δ_a. The time-averaged wall shear stress and frictional pressure gradient are calculated from Eq. (16). This semi-mechanistic estimate replaces the fully homogeneous flow calculation, in which equivalent fluid properties are employed in Eq. (18). As noted above, the time-averaged gravitational and acceleration components of the pressure gradient are still calculated from the homogeneous flow model.

A mechanistic model for confined-bubble flow should not be applied to any other flow regime but the model does not define its own limits. The assumption of phase equilibrium implies that the single nucleation site coincides with x = 0 and that a bubble of negligible length instantly fills the channel. The wall superheat required for nucleation and the motion of bubbles before confinement are not considered.

The assumption that the transport of liquid in the film is negligible implies that the liquid plug between confined bubbles remains until x = 1. The mean velocity in the film is given by

$$\bar{u} = \frac{\tau_i}{2\mu_l}\delta_m - \left[\frac{dp}{dz} + \rho_l g\right] \frac{\delta_m^2}{3\mu_l} \quad (24)$$

A sufficient condition for the disappearance of the liquid slug is that the liquid film transports the entire liquid flow corresponding to the value of *x* based on thermal equilibrium:

$$\rho_l \bar{u} \delta_m \frac{t_e}{t_b} = \frac{DG(1-x)}{4} \quad (25)$$

but the regime of confined bubbles with smooth laminar films may well break down at smaller values of *x* due to wave formation on the films or instability of the ends of the liquid plug between bubbles.

5. PREDICTION OF DRYOUT VAPOR QUALITY FOR ANNULAR TWO-PHASE FLOW IN MICRO-CHANNELS

Flow boiling heat transfer in so-called microchannels is now the hottest topic in heat transfer research, as the need has arisen for very high heat flux cooling for the new generation of computer chips. Heat flux dissipation rates have risen from about 30 W/cm^2 just a few years ago to 100 W/cm^2 today, and the challenge is now to arrive at 300 W/cm^2 and higher in the near future (written in units used by the electronics industry). The last challenge represents a heat flux that is considerably beyond the experience of macroscale flow boiling. Flow Boiling is attractive over single phase liquid cooling because of high heat transfer coefficient and higher heat removal capability for a given mass flow rate of the coolant. Flow boiling systems can carry large amount of thermal energy through latent heat of vaporization.

$$\frac{\partial}{\partial t}\left(\alpha_v \rho_v c_{pv} \boldsymbol{T}_v\right) + \boldsymbol{\nabla}.\left(\alpha_v \rho_v c_{pv} \boldsymbol{V}_v \boldsymbol{T}_v\right) = \boldsymbol{\nabla}.\left(k_v' \nabla \boldsymbol{T}_v\right) + \alpha_v \frac{\partial \boldsymbol{P}}{\partial \boldsymbol{T}} + \boldsymbol{q_{lv}} + \Gamma_{lv} h_l$$

$$\frac{\partial}{\partial t}\left(\alpha_l \rho_l c_{pl} \boldsymbol{T}_l\right) + \boldsymbol{\nabla}.\left(\alpha_l \rho_l c_{pl} \boldsymbol{V}_l \boldsymbol{T}_l\right) = \boldsymbol{\nabla}.\left(k_l' \nabla \boldsymbol{T}_l\right) + \alpha_l \frac{\partial \boldsymbol{P}}{\partial \boldsymbol{T}} + \boldsymbol{q_{vl}} + \Gamma_{vl} h_v$$

$$Q = h_{lv} A_{lv} (T_v - T_l) \quad \alpha_v + \alpha_l = 1$$

$$\frac{\partial V_l}{\partial x} = \frac{\partial V_g}{\partial x} = \frac{\partial \alpha_l}{\partial x} = \frac{\partial \alpha_g}{\partial x} = \frac{\partial T}{\partial x} = 0$$

$$V_{bx} = \frac{8(T_1 - T_{sat})^2 k_l^2}{h_{fg}^2 \rho_l^2 d_{BW}} \left(\frac{3}{\pi \beta_l}\right)$$

$$d_{BW} = 0.208\phi \sqrt{\frac{\sigma}{g(\rho_l - \rho_g)}}$$

$$a_v = \frac{\pi n f d_{BW}^3}{V_{bx}}$$

$$N = [210(T_w - T_{sat})]^{1.805}, \quad f = 0.9\sqrt{\frac{g}{d_{Bw}}}$$

$$Q_e = nf\left(\frac{\pi}{6} d_{BW}^3\right) \rho_g h_{fg}$$

$$Q_q = (\frac{2}{\sqrt{\pi}}\sqrt{K_l \rho_l C_{pl}}\sqrt{f}) A_q (T_w - T_l)$$

$$A_q = \text{nK}\ (\frac{\pi d_{BW}^2}{4})$$

$$Q_c = \text{St}\ \rho_l \boldsymbol{C}_{pl} \boldsymbol{V}_l (T_w - T_l)(1 - A_q)$$

$$\text{St} = \frac{N_u}{RePr}$$

$$a_P \emptyset_P = a_E \emptyset_E + a_W \emptyset_W + a_N \emptyset_N + a_S \emptyset_S + b$$

$$\text{q} = Q_e + Q_q + Q_c$$

From a historical perspective, microchannels are currently at an infancy stage. We are still trying to understand their characteristics. Their widespread usage is expected to begin with advances in MEMS devices and systems, microscale sensors and actuators, advanced high heat flux removal systems, and biomedical applications. As an example, the use of microchannels and nanochannels is critical in developing highly efficient heat and mass transfer devices, such as artificial kidneys or lungs suitable for human implant. These developments are expected to make headlines in the coming decades.

Kandlikar[1] proposed the following correlation for channel classification based on hydraulic diameter.

Conventional channels: >3 mm

Minichannels: 3 mm>Dh >200 µm

Microchannels: 200 µm > Dh >10 µm

Transitional Channels: 10 µm > Dh > 0.1 µm ~100 nanometer, nm, or 1000 Å

Transitional Microchannels: 10 µm >Dh >1 µm

Transitional Nanochannels: 1 µm>Dh>0.1 µm

Molecular Nanochannels: 0.1 µm>Dh

6. EFFECT OF WALL THICKNESS

The influence of surface finish and tube wall thickness on the critical heat flux. It is possible to list four secondary variables associated with the test section which, so far, have not been considered. These are:
(i) method of heating the tube
(ii) material of the tube wall
(iii) tube wall thickness
(iv) internal bore surface finish.

$$\frac{1}{r}\left(r\frac{\partial T}{\partial r}\right) + \frac{1}{r2}\left(\frac{\partial^2 T}{\partial \varphi^2}\right) = 0$$

$$\frac{\partial T(r,\varphi)}{\partial \varphi} = \frac{\partial T(r,\varphi+2\pi)}{\partial \varphi}$$

$$T(r,\varphi) = T(r,\varphi+2\pi)$$

$$K_w \cdot \frac{\partial T(r_i,\varphi)}{\partial r} = \begin{cases} h_g\left(T(r_i,\varphi) - T_{sat}\right) : 0 \le \phi \le \varphi_0 \\ h_f\left(T(r_i,\varphi) - T_{sat}\right) : \varphi_0 \le \phi \le \pi \end{cases}$$

$$K_w \cdot \frac{\partial T(r_o,\varphi)}{\partial r} = \begin{cases} q^{0''}(\varphi) \\ 0 : \frac{\pi}{2} \le \phi \le \pi \end{cases} : 0 \langle \phi \le \frac{\pi}{2}$$

To this list might be added the method used for detection of the critical heat flux. Since an accurate correlation of the available world data has been achieved without the inclusion of the above factors as independent variables, it seems reasonable to conclude that they do not play a significant role in the determination of the critical heat flux value. However, few systematic investigations of the importance of these variables have been undertaken. The experimental critical heat flux data listed by Macbeth and Thompson were taken using Joule heating of the test channel. Most experiments used direct current heating. It has been suggested (Bertoletti et al. 1 959; Tippets 1962) that the use of alternating current with test elements having a low thermal capacity and short time constant causes a reduced critical heat flux, all other independent variables remaining fixed. Aladyev et al. (1961) report that the thickness of the tube wall did not affect the critical heat flux in the range 0.0 1 6 to 0.079 in. Barnett (1963) suggests that some influence of tube wall thickness might explain an apparent slight inconsistency in the data of Lee and Obertelli (1963). Data taken at AERE Harwell and AEE Winfrith (Lee 1965) suggest that there is a small reduction in the critical heat flux ('" 5 per cent) at low inlet subcoolings as the tube wall thickness is decreased from 0.084 to 0.034 in, all other independent variables remaining constant. Tippets (1962) reports a decrease in critical heat flux of approximately 20 per cent when a 0.01 0 in thick ribbon heater was replaced by a 0.006 in thick ribbon. Some influence of tube wall thickness might be expected by comparison with the influence of this variable in pool boiling experiments. There appears to be some difference of opinion on the influence of tube wall material and internal bore surface finish. It should be observed that for the purposes of this discussion '

roughness ' refers to the ' micro-roughness ' of normal machined engineering surfaces. The influence of certain types of macro-roughness will be considered in Chapter 1 1 . De Bortoli et al. (1963) concluded that the heat transfer surface material or roughness of the surface did not influence the critical heat flux. The materials investigated were nickel, Zircaloy II, and stainless steel. With Zircaloy II two surface roughness values were investigated, namely 29 micro inches and 1 20 microinches. Aladyev et al. (1961) report no influence of surface finish on the critical heat flux. In these experiments eleven tubes with various internal finishes were tested, including polished, etched, and machined surfaces. The evidence for some effect of surface finish comes from the data of Weatherhead (1963) in the USA and Chirkin and Iukin (1 956) in the U SSR. Both of these works conclude that the critical heat flux is lowered for very smooth surfaces upon which bubble nucleation might be difficult. It has been reported that porous deposits on heat transfer surfaces can influence the critical heat flux both favourably and adversely. In tests reported by Goldstein et al. (1967) the addition of contaminants to a test circuit caused reductions in the critical heat flux. The effect was temporary and the critical heat flux value returned to the clean tube figure after a period of several hours.

$$\frac{1}{r*}.\frac{\partial}{\partial r*}\left(r*\frac{\partial\theta}{\partial r*}\right)+\frac{1}{r*^2}.\frac{\partial^2\theta}{\partial\varphi^2}=0$$

$$\frac{\partial\theta(r*,\varphi)}{\partial\varphi}=\frac{\partial\theta(r*,\varphi+2\pi)}{\partial\varphi}$$

$$\theta(r*,\varphi)=\theta(r*,\varphi+2\pi)$$

$$\frac{\partial\theta(1,\varphi)}{\partial r*}=\begin{cases}Bi_g.\theta(1,\varphi):0\le\phi\le\phi_0\\ Bi_f.\theta(1,\varphi):\phi_0\le\phi\le\pi\end{cases}$$

$$\frac{\partial\theta(r_0*,\varphi)}{\partial r*}=\begin{cases}q*(\varphi):0\le\phi\le\frac{\pi}{2}\\ 0:\frac{\pi}{2}\le\phi\le\pi\end{cases}$$

$$\frac{1}{r*}.\frac{\partial}{\partial r*}\left(r*.\frac{\partial\theta_1}{\partial r*}\right)+\frac{1}{r^{*2}}.\frac{\partial^2\theta_1}{\partial\varphi^2}=0$$

$$\theta_1(r*,\varphi)=\theta_1(r*,\varphi+2\pi)$$

$$\frac{\partial\theta_1(r*,\varphi)}{\partial\varphi}=\frac{\partial\theta_1(r*,\varphi+2\pi)}{\partial\varphi}$$

$$\frac{\partial\theta_1(1,\varphi)}{\partial r*}=Bi_g.\theta_1(1,\varphi)$$

$$\frac{\partial\theta_1(r_0*,\varphi)}{\partial r*}=\begin{cases}q*(\varphi):0\le\phi\le\frac{\pi}{2}\\ 0:\frac{\pi}{2}\le\phi\le\pi\end{cases}$$

$$\frac{1}{r*}.\frac{1}{\partial r*}\left(r*\frac{\partial\theta_2}{\partial r*}\right)+\frac{1}{r*^2}.\frac{\partial^2\theta_2}{\partial\varphi^2}=0$$

$$\theta_2(r*,\varphi)=\theta_2(r*,\varphi+2\pi)$$

$$\frac{\partial\theta_2(r*,\varphi)}{\partial\varphi}=\frac{\partial\theta_2(r*,\varphi+2\pi)}{\partial\varphi}$$

$$\frac{\partial\theta_2(r_0*,\varphi)}{\partial r*}=0$$

$$\frac{\partial\theta_2(1,\varphi)}{\partial r*}=\begin{cases}Bi_g\theta_2(1,\varphi):0\le\phi\le\phi_0\\ (Bi_f-Bi_g)[\theta_1(1,\varphi)+\theta_2(1,\varphi)]+\\ Bi_g.\theta_2(1,\varphi):\varphi_0\le\phi\le\pi\end{cases}$$

since

$$b_0=\frac{r_0*}{Bi_g}\int_0^\pi q*(\varphi)\,d\varphi$$

$$b_n=\int_0^\pi q*(\varphi)\cos n\varphi d\varphi/\left\{n\left(\frac{n+Bi_g}{n-Bi_g}r_0*-r_0*\right)\right\}$$

which has

$$\theta_1=\frac{r_0*}{2}\left(\ln r*+\frac{1}{Bi_g}\right)+\sum_{n=1}^{\infty}p(r*,n)\cos n\varphi$$

$$p(r*,n)=\frac{2r_0*}{\pi n^2}.\frac{H(n)r*^n+r*^{n-1}}{H(n)r_0*^n-r_0*^{n-1}}.\sin\frac{n\pi}{2}$$

$$H(n)=\frac{n+Big}{n-Big}$$

$$\theta_1=\frac{r_0*}{\pi}\left(Lnr*+\frac{1}{Bi_g}\right)+$$

$$p'(1,1)\cos\phi+\sum_{n=2}^{\infty}p'(r*,n)\cos n\phi$$

$$p'(r*,1)=\frac{r_0*}{2}.\frac{H(1)r*+\frac{1}{r*}}{H(1)r_0*-\frac{1}{r_0*}}$$

$$p'(r^*,n)=\frac{r_0^*}{\pi n}\cdot\frac{H(n)r^{*n}+r^{*-n}}{H(n)r_0^{*n}-r_0^{*-n}}\left[\frac{\sin(n-1)\frac{\pi}{2}}{n-1}+\frac{\sin\left(n+1\frac{\pi}{2}\right)}{n+1}\right]$$

$$0=\pi A+\left(\frac{Bif}{Big}-1\right)\left\{\left(A+\frac{r_0^*}{2Big}\right)(\pi-\varphi_0)-\sum_{n=1}^{\infty}\left[b_n\left(r_0^{*-2n}+1\right)+p(1,n)\right]\frac{1}{n}\sin n\varphi_0\right\}$$

$$\frac{\pi}{2}b_m\left[r_0^{*-2m}-\frac{m+Big}{m-Big}\right]=\frac{Bif-Big}{m-Big}-\left\{-\left(A+\frac{r_0^*}{2Big}\right)\left(\frac{Bif}{Big}-1\right)(\pi-\varphi_0)\right\}$$

$$\sum_{n=1}^{\infty}\left[b_n\left(r_0^{*-2n}+1\right)+p(1,n)\right]\int_{\varphi_0}^{\pi}\cos n\varphi\cos m\varphi d\varphi$$

then the matrix would be

$$A.\chi=B$$

$$A=\begin{bmatrix}a_{1,1}a_{1,2}.....a_{1,p+1}\\ a_{2,1}a_{2,2,}.....a_{2,p+1}\\ a_{3,1}a_{3,2}.....a_{3,p+1}\\ .....\\ .....\\ a_{p+1,1}a_{p+1,2}.....a_{p+1,p+1}\end{bmatrix}$$

$$X=\begin{bmatrix}A\\ b_1\\ b_2\\ b_3\\ .\\ .\\ .\\ .\\ .b_p\end{bmatrix}$$

$$B=\begin{bmatrix}a_{1,p+2}\\ a_{2,p+2}\\ a_{3,p+2}\\ .\\ .\\ .\\ a_{p+2,p+2}\end{bmatrix}$$

$$a_{1,n+1}=-\left(\frac{Bi_f}{Bi_g}-1\right)\left(r_0^{*-2n}+1\right)\frac{1}{n}\sin n\varphi_0$$

$$a_{1,p+2}=-\left(\frac{Bif}{Big}-1\right)\left[\frac{r_0^*}{2Big}(\pi-\varphi_0)-\sum_{n=1}^{p}p(1,n).\frac{1}{n}\sin n\varphi_0\right.$$

$$a_{m+1,1}=-\frac{Bif-Big}{m-Big}.\frac{1}{m}\sin m\varphi_0$$

$$a_{m+1,n+1}=\frac{Bif-Big}{m-Big}\left(r_0^{*-2m}+1\right)$$

$$\left[\frac{1}{2}(\pi-\phi_0)-\frac{\sin 2m\phi_0}{4m}\right]$$

$$-\frac{\pi}{2}\left[r_0^{*-2m}-\frac{m+Big}{m-Big}\right]$$

$$=-\frac{Bif-Big}{m-Big}\left(r_0^{*-2m}+1\right)$$

$$\left[-\frac{\sin(m-n)\phi_0}{2(m-n)}-\frac{\sin(m+n)\phi_0}{2(m+n)}\right]$$

$$a_{m+1,p+2} = -\frac{Bif\ -Big}{m-Big}$$

$$\left[\begin{array}{l} \frac{r_0\,*}{2Big}.\frac{1}{m}\sin(-m\phi_0)+ \\ \quad p(1,n)= \\ \sum_{n=1}^{p}\begin{cases}\frac{1}{2}(\pi-\phi_0)-\frac{\sin(2m\phi_0)}{4m}:m=n \\ -\frac{\sin(n-m)\phi_0}{2(n-m)}-\frac{\sin(n+m)}{2(n+m)}:m\neq n\end{cases}\end{array}\right]$$

$$0=\pi A+\left(\frac{Bif}{Big}-1\right)$$

$$\left\{\begin{array}{l}\left(A+\frac{r_0\,*}{\pi Big}\right)(\pi-\phi_0) \\ -\left[p'(1,1)+b_1\left(r_0\,^{*-2}+1\right)\right].\sin\phi_0 \\ -\sum_{n=2}^{\infty}\left[b_n\left(r_0\,^{*-2n}+1\right)+p'(1,n)\right]\frac{1}{n}\sin n\phi_0\end{array}\right\}$$

$$\frac{\pi}{2}b_m\left[r_0\,^{*-2m}-\frac{m+Big}{m-Big}\right]=\frac{Bif\ -Big}{m-Big}.F$$

$$F=\left\{\begin{array}{l}-\left(A+\frac{r_0\,*}{\pi Big}\right)\frac{1}{m}\sin m\phi_0 \\ +\left[p'(1,1)+b_1\left(r_0\,^{*-2}+1\right).S+L\right]\end{array}\right\}$$

$$S=\begin{cases}-\frac{\sin(m-1)\varphi_0}{2(m-1)}-\frac{\sin(m+1)\varphi_0}{2(m+1)}:m\neq 1 \\ \frac{1}{2}(\pi-\varphi_0)-\frac{1}{4}\sin 2\varphi_0:m=1\end{cases}$$

$$L=\sum_{n=2}^{\infty}\left[b_n\left(r_0\,^{*-2m}+1\right)+p'(1,n)\right].S$$

$$a_{1,1}=\pi+\left(\frac{Bif}{Big}-1\right)(\pi-\varphi_0)$$

$$a_{1,2}=-\left(\frac{Bif}{Big}-1\right)\left(r_0\,^{*-2}+1\right)\sin\varphi_0$$

$$a_{1,n+1}=-\left(\frac{Bif}{Big}-1\right)\left(r_0\,^{*-2n}+1\right)\frac{1}{n}\sin n\varphi_0$$

$$a_{1,p+2}=-\left(\frac{Bif}{Big}-1\right)\left[\begin{array}{l}\frac{r_0\,*}{\pi}.\frac{\pi-\phi_0}{Big}-p'(1,1)\sin\phi_0 \\ -\sum_{n=1}^{p}p'(1,n)\frac{1}{n}\sin n\phi_0\end{array}\right]$$

$$a_{m+1,1}=-\frac{Bif\ -Big}{m-Big}.\frac{1}{m}\sin m\varphi_0$$

$$a_{m+1,2}=\frac{Bif\ -Big}{m-Big}\left(r_0\,^{*-2}+1\right)$$

$$*\left\{\begin{array}{l}-\frac{\sin(m-1)\phi_0}{2(m-1)}-\frac{\sin(m+1)\phi_0}{2(m+1)} \\ \frac{1}{2}(\pi-\phi_0)-\frac{\sin 2\phi_0}{4}\end{array}\right.$$

$$a_{m+1,n+1}=\frac{Bif\ -Big}{m-Big}\left(r_0\,^{*-2m}+1\right)$$

$$\left[\frac{1}{2}(\pi-\phi_0)-\frac{\sin 2m\phi_0}{4m}\right]$$

$$-\frac{\pi}{2}\left[r_0\,^{*-2m}-\frac{m+Big}{m-Big}\right]:n=m$$

$$a_{m+1,n+1}=\frac{Bif\ -Big}{m-Big}\left(r_0\,^{*-2m}+1\right)\left[-\frac{\sin(n-m)\varphi_0}{2(n-m)}-\frac{\sin(n+m)}{2(n+m)}\right]:m\neq n$$

$$a_{m+1,p+2}=\frac{-(Bif\ -Big)}{m-Big}$$

$$\left[-\frac{r_0\,*}{\pi Big}.\frac{1}{m}\sin m\phi_0+p'(1,1)S+I\right]$$

$$I=\sum_{n=2}^{p}p'\left(1,n\int_{\varphi_0}^{\pi}\cos n\varphi.\cos m\varphi d\varphi\right)$$

7. DRYOUT POSITION PREDICTION

A mechanistic model of post dryout heat transfer has been developed involving momentum and energy equations for both vapor and liquid, average drop diameter at the dryout location, and using heat transfer correlations for vapor-to-drop, wall-to-drop, and wall-to-vapor. This involves a computer calculation stepwise down the tube from dryout. This calculation was simplified making possible the heat transfer prediction at any position down the tube without the stepwise solution. The two solutions agree well with each other. To make the predictions agree with data it was found necessary to multiply the wall-to-vapor heat transfer coefficient by a factor ranging from around 0.7 to about 2. At present this factor is found to be a

function of bulk to wall viscosity ratio and quality. It may also be a function of liquid and vapor densities, tube and particle diameters and Reynolds number. A similar effect of wall-to-gas heat transfer is found in solid particle-gas flowing mixtures. The detailed explanation is as yet unknown, but appears to be due to turbulence suppression and enhancement resulting from particle motion

$$\left(\dot{M}'+\Delta\dot{M}'\right)R\Delta\theta+\left(\dot{N}'+\Delta\dot{N}'\right)\Delta Z$$
$$+\dot{m}''R\Delta\theta\Delta Z-\left(\dot{M}'R\Delta\theta+\dot{N}'\Delta Z\right)=0$$

As it was already mentioned, during film dry-out the film entrainment and deposition model play a very important role. The source of entrainment mass rate is defined as

$$\frac{\partial\dot{M}'(Z,\theta)}{\partial q}+\frac{1}{R}\cdot\frac{\partial\dot{N}'}{\partial\theta}+\dot{m}''=0$$

The net source of entrainment mass rate S is the net result of the opposing mechanisms of entrainment, S& and de-entrainment SD& In film flow there are two models describing the entrainment, one for a counter-current situation and another one for the co-current case. In a co-current flow scenario the mechanism is described as the development of low-amplitude roll waves at the film with drops being sheared off the wave crest. In a counter-current scenario there are typically large amplitude waves, which abruptly break leading to liquid entrainment.

$$\dot{m}''=\frac{\dot{q}''(\theta)}{h_{fy}}+\dot{m}_e''-\dot{m}_d''$$

The model used for the counter-current case is the following. The entrainment rate is taken to be the difference between the liquid flow rate in the film and the critical film flow rate:

$$\frac{\partial\dot{M}'}{\partial Z}+\frac{1}{R}\frac{\partial\dot{N}'}{\partial\theta}+\frac{\dot{q}''}{h_{fy}}+\dot{m}_e''-\dot{m}_d''=0$$

where the critical void fraction is calculated from a force balance between the disruptive force of the pressure gradient over the crest of waves on the film and the restraining force of surface tension. The expression for the critical film thickness is

$$\dot{N}'=-\frac{S}{R}\frac{\partial\dot{M}'}{\partial\theta}$$

It is assumed that all liquid in excess of that required for a stable film is removed from the film and enters into the entrained liquid field. The model used for co-current flow is based on the Whalley, Hewitt and Hutchinson correlation. The entrainment is proportional to the interfacial shear stress and inversely proportional to the surface tension. The resulting entrainment rate is given as:

$$\frac{\partial\dot{M}'}{\partial Z}-\frac{S}{R^2}\frac{\partial^2\dot{M}'}{\partial\theta^2}+\frac{\dot{q}''(\theta)}{h_{fy}}+\dot{m}_e''-\dot{m}_d''=0$$

Tatterson et al. [8] have characterized the size of the droplets formed by entrainment from films. His results are used for both counter-current and co-currentflow:

$$q''(\theta)=\frac{q''}{\pi}\left[1+\frac{\pi}{2}\cos\theta+\sum_{n=2}^{\infty}\alpha(n)\cos\theta\right]$$

The deposition of drops on the liquid film occurs as result of random turbulent motions. The rate of deposition is calculated with the Cousins' model [9]. This is a diffusion model where the deposition rate is assumed proportional to the drop concentration gradient, which is assumed to be zero at the wall. The de-entrainment rate is given as:

$$\alpha(n)=\frac{\sin(n+1)\frac{\pi}{2}}{n+1}+\frac{\sin(n-1)\frac{\pi}{2}}{n-1}$$

It is important to note that the previous models and correlations have been developed from single tube data, not rod bundle data.

$$\dot{m}_d''=A-BX$$

In a system where a liquid film flow along the wall with a gas phase flowing over it, several hydrodynamic transitions leading to entrainment of some of the liquid as droplets are possible. At certain relative velocity interfacial waves appear and as the relative velocity is increased these dynamic waves can transform to large amplitude roll waves which propagate in one direction. At the roll wave transition or at a slightly higher gas velocity, the onset of entrainment has been observed.

$$\dot{m}_e''=\frac{4B\dot{M}'}{D\cdot G}$$

There are several different entrainment mechanisms, and it has been observed that the onset of entrainment can depend on the flow directions.

By considering these possibilities detailed criteria for onset of entrainment have been developed. For the annular flow of low viscous fluids such as water or sodium, the entrainment mechanism based on the shearing-off of roll wave crests is the predominant mode. The onset of entrainment occurs when the retaining force of surface tension is exceeded by the interfacial shear force exerted by the streaming gas flow.

$$X = \frac{2q''}{\pi RGh_{fy}} \cdot Z$$

Transient critical heat flux (CHF) has received much attention recently particularly when associated with the safety analysis of water reactors. The transients are of many types. Power excursions, depressurisation, loss of fluid, pump coast down, flow reversal etc. have all received considerable attention.

$$\frac{\partial \dot{M}'}{\partial Z} - \frac{S}{R^2} \cdot \frac{\partial^2 \dot{M}'}{\partial \theta^2} + \frac{2B}{RG} \cdot$$

This inception criterion is given in a non-dimensional form by

$$\frac{\partial \dot{M}'}{\partial Z} - \frac{S}{R^2} \cdot \frac{\partial^2 \dot{M}'}{\partial \theta^2} + \frac{2B}{RG} \cdot \dot{M}' = A - \frac{2Bq''}{\pi h_{fy} \cdot R \cdot G} Z - \frac{q''}{\pi h_{fy}} \left\{ 1 + \frac{\pi}{2} \cos\theta + \sum_{n=2}^{\infty} \alpha(n) \cos\theta \right\}$$

Although there are considerable scattering of data around the criterion, mainly due to different techniques used for different data and also due to the inclusion of data for highly viscous fluids, the overall trend is well predicted. The important parameter concerning the entrainment is the amount of liquid flowing as droplets. This can be considered in terms of the fraction of liquid flux entrained which is defined by

$$\dot{M}_i' = \frac{\pi R^2 G - \frac{2q''RL}{h_{fy}}}{2\pi R}$$

Furthermore, by considering the effect of increased inertia of gas core flow due to the existence of droplets and the effect of droplet deposition, basic dimensionless parameters have been identified. It has been found that the fully developed entrainment depends on three dimensionless groups given by

$$\frac{\dot{M}_0'}{Z_0} \cdot \frac{\partial M}{\partial Z} - \frac{S}{R^2} \cdot \dot{M}_{0-}' \frac{\partial^2 M}{\partial \theta^2} + \frac{2B}{RG} \cdot \dot{M}_0' \cdot M + \frac{2B}{RG} \cdot \dot{M}_i' = -\frac{q''}{\pi h_{fy}} \left\{ 1 + \frac{\pi}{2} \cos\theta + \sum_{n=2}^{\infty} \alpha(n) \cos n\theta \right\} + A - \frac{2Bq''z_0}{\pi h_{fy} \cdot R \cdot G} Z_0$$

$$\frac{SZ_0}{R^2} = 1$$

The entrained fraction reaches a quasi-equilibrium value, E, at points far removed from the tube entrance where the entrainment and deposition processes attain an equilibrium condition. The distance necessary to reach this condition is approximately by

$$\frac{q''}{\pi h_{fy}} \cdot \frac{z_0}{\dot{M}_0'} = 1$$

It is noted that the above expression is given in terms of the Weber number and total liquid Reynolds number. As can be seen here, if the Weber number is used, the significant length scale is Dh. Then the Taylor wavelength scale, which is the standard length scale for interfacial phenomena, does not appear in the correlation.

$$Z_0 = \frac{R^2}{S}$$

$$\dot{M}_0' = \frac{R^2 q''}{\pi h_{fy} \cdot s}$$

$$M = M_P + M_h$$

$$M_h = \sum_{n=0}^{\infty} a_n \left[1 - \exp\left[-\left(n^2 + \frac{2BR}{GS} \right) Z \right] \right] \cos n\theta$$

In many two-phase flow formulations the droplet volumetric concentration in the gas core alone is very important. It is defined by

$$M_P = f(\theta) + g(z)$$

Then the above equilibrium entrainment fraction correlation can be rewritten approximately as

$$M_P = \frac{GR}{2B}\left[\frac{A}{\dot{M}'} - \frac{\dot{M}_i'}{\dot{M}'}\cdot\frac{2B}{GR}\cdot Z\right] - \frac{\frac{\pi}{2}\cos\theta + \sum_2^\infty \alpha'\cdot\alpha\cos n\theta}{1+\frac{2B}{GR}Z_0}$$

Some experimental data indicated the strong entrance effect as well as the gas expansion effect due to the axial pressure drop in a low pressure system. For the correlation development it was essential to use a local gas velocity or volumetric flux based on a local pressure in evaluating data.

$$\alpha'(n) = \frac{1+\frac{2B}{GR}Z_0}{n^2+\frac{2B}{GR}Z_0}$$

$$a_0 = \frac{-GR}{2B}\cdot\frac{A}{\dot{M}_0'}$$

$$a_1 = \frac{\frac{\pi}{2}}{1+\frac{2B}{GR}Z_0}$$

$$a_n = \frac{\alpha'(n)\alpha(n)}{1+\frac{2B}{GR}Z_0} \quad n \geq 2$$

A number of data from the entrance region have been successfully correlated by this expression. This inclusion of entrance effect in the correlation is a significant improvement over the conventional correlations for the entrainment fraction. It can be observed that the fraction of liquid in the entrance region can be significantly smaller than that in the fully developed regime, if the liquid flow starts as a film flow at the entrance.

In boiling two-phase flow the entrance effect on the annular flow itself can" be neglected. Thus these two equations can be used for an annular dispersed flow following a boiling section. In an adiabatic flow, the above mentioned entrance effect should be considered.

A correlation for the entrainment fraction or droplet volumetric fraction correlation gives direct information on the amount of droplet flow in terms of macroscopic variables. Therefore, it is not necessary to introduce droplet and film flow field equations. In particular, it is not necessary to use separate continuity and momentum equations for droplets and film. Thus the use of the above correlations is consistent with the mixture model such as the drift-flux model

$$M = \frac{GR}{2B}\left\{\frac{A}{\dot{M}_0'}\left[1-\exp\left[-\frac{2BR}{GS}Z\right]\right]\right\} - \left\{\frac{\dot{M}_i'}{\dot{M}_0'} - \frac{\frac{\pi}{2}}{1+\frac{2B}{GR}Z_0}\left\{1-\exp\left[-\left(1+\frac{2BR}{GS}\right)Z\right]\right\}\right\}\cos\theta - \frac{\sum_2^\infty \alpha'(n)\alpha(n)\left\{1-\exp\left[-\left(n^2+\frac{2BR}{GS}Z\right)\right]\right\}\cos\theta}{1+\frac{2B}{GR}Z_0}$$

The interfacial area in annular dispersed flow can be expressed as

$$\overline{m}_d'' = k\cdot c$$

where

$$c = \frac{eGL}{e\frac{GL}{\rho L}+\frac{Gg}{\rho g}}$$

$$c = \rho g\cdot\frac{1-x}{x}\cdot e$$

$$e = 0\cdot 8187\frac{XG}{\rho g}$$

$$c = 0.8187G(1-x)$$

The entrainment and deposition rates specify the liquid mass transfer between the liquid film and entrained droplet fields. Therefore, in order to properly use these rate correlations in a two-phase flow formulation, it is necessary to introduce two liquid fields.

$$\dot{m}_d'' = 0.8187kG(1-x)$$

where

$$A = B = 0.8187KG$$

and

$$K = 9.48\times10^4\sigma^{4.7}$$

$$L_{DO} = \frac{RGA}{2\dot{M}_0' B} - \frac{\frac{\pi}{2} + \sum_{2}^{\infty} \alpha(n)\alpha'(n)}{1 + \frac{2B}{RG} \cdot Z_O}$$

$$L_{DO} = \frac{RG}{2\dot{M}_0'} - \frac{\frac{\pi}{2} + \sum_{2}^{\infty} \alpha(n)\alpha'(n)}{1 + \frac{2B}{RG} \cdot Z_0}$$

8. REFERENCES

1. T.S. Bhatti, R.C. Bansal, and D.P. Kothari, "Reactive Power Control of Isolated Hybrid Power Systems", *Proceedings of International Conference on Computer Application in Electrical Engineering Recent Advances (CERA)*, Indian Institute of Technology Roorkee (India), February 21-23, 2002, pp. 626-632.
2. B.N. Singh, Bhim Singh, Ambrish Chandra, and Kamal Al-Haddad, "Digital Implementation of an Advanced Static VAR Compensator for Voltage Profile Improvement, Power Factor Correction and Balancing of Unbalanced Reactive Loads", *Electric Power Energy Research*, Vol. 54, No. 2, 2000, pp. 101-111.
3. J.B. Ekanayake and N. Jenkins, "A Three-Level Advanced Static VAR Compensator", *IEEE Transactions on Power Systems*, Vol. 11, No. 1, January 1996, pp. 540-545.
4. Abdollahzadeh Jamalabadi, M.Y. (2015). Effects of micro and macro scale Viscous Dissipations with Heat Generation and Local Thermal Non-Equilibrium on Thermal Developing Forced Convection in saturated porous media, *Journal of Porous Media*, 18(9), 843-860.
5. Abdollahzadeh Jamalabadi, M.Y. (2015). Joule Heating in Low-Voltage Electroosmotic with Electrolyte containing nano-bubble mixtures through Microchannel Rectangular Orifice, *Chemical Engineering Research and Design*, 102, 407-415.
6. Abdollahzadeh Jamalabadi, M.Y., Ghasemi, M., & Hamedi, M.H. (2012). Two-dimensional simulation of thermal loading with horizontal heat sources, *Proceedings of the Institution of Mechanical Engineers, Part C: Journal of Mechanical Engineering Science*, 226, 1302-1308.
7. Abdollahzadeh Jamalabadi, M.Y., Park, J.H., & Lee, C.Y. (2015). Optimal Design of MHD Mixed Convection Flow in a Vertical Channel with Slip Boundary Conditions and Thermal Radiation Effects by using Entropy Generation Minimization Method, *entropy*, 17(2), 866-881.
8. Abdollahzadeh Jamalabadi, M.Y., & Park, J.H., (2014). Effects of Brownian motion on Freezing of PCM Containing Nanoparticles, *Thermal Science*, OnLine-First Issue, 00 94-94.
9. Abdollahzadeh Jamalabadi, M.Y., Park, J.H., & Lee, C.Y. (2014). Thermal Radiation effects on the Onset of Unsteadiness of Fluid Flow in Vertical Microchannel Filled with Highly Absorbing Medium, *Thermal Science*, OnLine-First Issue 00, 124-124.
10. Abdollahzadeh Jamalabadi, M.Y., Ghasemi M., & Hamedi M.H. (2013). Numerical Investigation of Thermal Radiation Effects on Open Cavity with Discrete Heat Sources, *International Journal of Numerical Methods for Heat and Fluid Flow*, 23(4), 649-661.
11. Abdollahzadeh Jamalabadi, M.Y. (2013). Electrochemical and exergetic modeling of a CHP system using tubular solid oxide fuel cell and mini gas turbine , *Journal of Fuel Cell Science Technology*, 10(5), 051007.
12. Abdollahzadeh Jamalabadi, M.Y. (2016). Optimal Design of Cylindrical PBX by Entransy Dissipation Extremum Principle, *International Journal of Energetic Materials and Chemical Propulsion*, accepted for publication, 15.

13. Abdollahzadeh Jamalabadi, M.Y. (2016). Thermal Radiation Effects on Creep Behavior of the Turbine Blade, *Multidiscipline Modeling in Materials and Structures*, minor revision.

14. Abdollahzadeh Jamalabadi, M.Y., Park, J.H., Rashidi, M.M., & Chen J.M. (2015). Effects of Thermal Boundary Conditions on the Joule Heating of Electrolyte in a Microchannel, *Journal of Hydrodynamics*, Ser. B, accepted for publication. DOI20:2010.1016/S1001-6058(16)60705-9

15. Abdollahzadeh Jamalabadi, M.Y., (2015). Entropy generation in boundary layer flow of a micro polar fluid over a stretching sheet embedded in a highly absorbing medium, *Frontiers in Heat and Mass Transfer*, 6(1), 1-13.

16. Abdollahzadeh Jamalabadi, M.Y. (2014). The frequency response of a cavitating hydrofoil, *Noise and Vibration Worldwide*, 45(8), 21-27.

17. [17] Abdollahzadeh Jamalabadi, M.Y. (2014). Analytical study of Magnetohydrodynamic propulsion stability, *Journal of Marine Science and Application*, 13(3), 281-290.

18. Abdollahzadeh Jamalabadi, M.Y. (2014). Experimental investigation of thermal loading of a horizontal thin plate using infrared camera, *Journal of King Saud University – Engineering Sciences*, 26(2), 159-167.

19. Abdollahzadeh Jamalabadi, M.Y., Park, J.H., & Lee, C.Y. (2014). Economic and environmental modeling of a micro gas turbine and solid oxide fuel cell hybrid combined heat and power system, *International Journal of Applied Environmental Sciences*, 9(4), 1769-1781.

20. Abdollahzadeh Jamalabadi, M.Y. (2014). Simulation of electrochemical impedance spectroscopy of a solid oxide fuel cell anodes, *World Applied Sciences Journal*, 32(4), 667-671.

21. Abdollahzadeh Jamalabadi, M.Y., & Park, J.H. (2014). Investigation of property variations on freezing of pcm containing nanoparticles, *World Applied Sciences Journal*, 32(4) 672-677.

22. Abdollahzadeh Jamalabadi, M.Y. (2014). Economic and environmental modeling of a MGT-SOFC hybrid combined heat and power system for ship applications, *Middle-East Journal of Scientific Research*, 22(4), 561-574.

23. Abdollahzadeh Jamalabadi, M.Y. (2015). MD simulation of Brownian motion on trapping of Buckminsterfullerene in nano-Optical tweezers, *International Journal of Optics and Applications*, 5(5), 161-167.

24. Abdollahzadeh Jamalabadi, M.Y. (2015). Numerical investigation of thermal radiation effects on electrochemical impedance spectroscopy of a solid oxide fuel cell anodes, *Materials Performance and Characterization*, DOI: 10.1520/MPC20140062.

25. Abdollahzadeh Jamalabadi, M.Y. (2015). Effect of fuel inject angle on the thermal behavior of a 2D axisymmetric non-premixed methane–air flame in vertical cylinder filled by porous media, *International Journal of Energy Engineering*, **5**,1, 1-8.

26. [26] Abdollahzadeh Jamalabadi, M.Y., & Park, J.H. (2014). Thermal radiation, joule heating, and viscous dissipation effects on mhd forced convection flow with uniform surface temperature, *Open Journal of Fluid Dynamics*, 4(2), 125-132.

27. Abdollahzadeh Jamalabadi, M.Y. (2014). Effect of fuel inject angle on non-premixed combustion of air/methane mixtures in vertical cylinder, International Journal of Multidisciplinary Research and Development, 1(5), 1-4.

28. Abdollahzadeh Jamalabadi, M.Y., & Park, J.H. (2014). Electro-Magnetic Ship Propulsion Stability under Gusts, *International Journal of Sciences: Basic and Applied Research Sciences*, 1, 421-427.

29. Abdollahzadeh Jamalabadi, M.Y., Hooshmand, P., Khezri, B., & Radmanesh,

A. (2014). Investigation of using different fluids for using in gas turbine- Rankine cycle, *Indian journal of Scientific Research*, 2, 74-81.

30. Bita, S., Abdollahzadeh Jamalabadi, M.Y., & Mesbah, M. (2015). Toxicity study of silver nanoparticles synthesized using seaweed Sargassum angustifolium in common carp, Cyprinus carpio, *Journal of Chemical and Pharmaceutical Research*, accepted for publication.

31. Dadgostari, F., Hosseininia, M. (2012). Phasing of Traffic Lights in Urban Intersections. *Graph Theory for Operations Research and Management: Applications in Industrial Engineering: Applications in Industrial Engineering*, 257.

32. Dousti, S., Cao, J., Younan, A., Allaire, P., & Dimond, T., (2012). Temporal and Convective Inertia Effects in Plain Journal Bearings With Eccentricity, Velocity and Acceleration, *Journal of tribology*, 134(3), 031704,8.
33. Dousti, S., & Fittro, R.L. (2015). An Extended Reynolds Equation Including the Lubricant Inertia Effects: Application to Finite Length Water Lubricated Bearings, *ASME Turbo Expo 2015: Turbine Technical Conference and Exposition.*
34. Dousti, S., Kaplan, J.A., He, F., & Allaire, P.E., (2013).Elastomer O-Rings as Centering Spring in Squeeze Film Dampers: Application to Turbochargers, *ASME Turbo Expo 2013: Turbine Technical Conference and Exposition*.
35. Dousti, S., Dimond, T.W., Allaire, P.E., & Wood, H.E. (2013). Time Transient Analysis of Horizontal Rigid Rotor Supported With O-Ring Sealed Squeeze Film Damper, *ASME 2013 International Mechanical Engineering Congress and Exposition.*
36. Dousti, S., Jalali, M.A., (2013). In-Plane and Transverse Eigenmodes of High-Speed Rotating Composite Disks, *Journal of Applied Mechanics*, 80(1), 011019.
37. Farahani, R.Z., Dadgostari, F., & Tirdad A. (2011). Future Trends in SCM.*Supply Chain Sustainability and Raw Material Management: Concepts and Processes: Concepts and Processes*, 82.
38. Farrokh, M, & Dizaji, M. S. (2015). Adaptive simulation of hysteresis using neuro-Madelung model, *Journal of Intelligent Material Systems and Structures*: 1045389X15604283.

39. He, F., Allaire, P.E., Dousti, & S., & Untaroiu, A. (2013). Forced response of a flexible rotor with squeeze film damper under parametric change, *ASME Turbo Expo 2013: Turbine Technical Conference and Exposition*, 1 (2013).

40. Hasani, R., Jafarzadeh, H., & Khoshalhan, F. (2013). A new method for supply chain coordination with credit option contract and customers' backordered demand. *Uncertain Supply Chain Management*, 1(4), 207-218.

41. Hassanzadeh, A., Mohseninezhad, L., & Tirdad, A., Dadgostari, F., Zolfagharinia, H. (2009). Location-routing problem. In Facility Location, 395-417. Physica-Verlag HD.

42. Hosseininia, M., & Dadgostari, F. (2013). Connectivity. *In R. Farahani, & E. Miandoabchi (Eds.) Graph Theory for Operations Research and Management: Applications in Industrial Engineering*, 37-47, Hershey, PA: Business Science Reference. doi:10.4018/978-1-4666-2661-4.ch004.
43. Hosseininia, M., & Dadgostari, F. (2012). Hamiltonian Paths and Cycles. In *Graph Theory for Operations Research and Management: Applications in Industrial Engineering: Applications in Industrial Engineering*, 96.
44. Jafarzadeh, H., Gholami, S., & Bashirzadeh, R. (2014). A new effective algorithm for on-line robot motion planning. *Decision Science Letters*, **3**, 1, 121-130.

45. Joghataie, A., & Dizaji, M.S. (2009). Nonlinear analysis of concrete gravity dams by neural networks, *In Proceedings of the World Congress on Engineering*, 2.
46. Joghataie, A., & Dizaji, M.S. (2012). Designing High-Precision Fast Nonlinear Dam Neuro-Modelers and Comparison with Finite-Element Analysis, *Journal of Engineering Mechanics*, 139(10), 1311-1324.

47. Joghataie, A., & Dizaji, M.S. (2010). Transforming results from model to prototype of concrete gravity dams using neural networks." *Journal of Engineering Mechanics*.
48. Joghataie, A., & Dizaji, M.S. (2010). Reducing extent of cracks and increasing time to failure of concrete gravity dams by optimization of properties of layers of concrete." *Scientia Iranica. Transaction A, Civil Engineering*, 21.1 67.
49. Kaplan, J. A., Dousti, S., Allaire, P. E., & Nichols, B. R., Dimond, T. W., & Untaroiu, A. (2013). Rotor Dynamic Modeling of Gears and Geared Systems. *In ASME Turbo Expo 2013: Turbine Technical Conference and Exposition.*
50. Sarshari, E., Vasegh, N., Khaghani, M., & Dousti, S. (2013). Sliding Mode Control in Ziegler's Pendulum With Tracking Force: Novel Modeling Considerations, *ASME 2013 International Mechanical Engineering Congress and Exposition.*
51. Shahidian, A., Ghassemi, M., Khorasanizade, S., Abdollahzade, M., & Ahmadi, G. (2009). Flow Analysis of Non-Newtonian Blood in a Magnetohydrodynamic Pump, *IEEE Transactions on Magnetics*, 45(6), 2667-2670.
52. Shadloo, M. S., Poultangari, R., Abdollahzadeh Jamalabadi, M.Y., & Rashidi, M.M. (2015). A New and Efficient Mechanism for Spark Ignition Engines, *Energy Conversion and Management*, 96, 418-429.
53. J.M.H. Peters, J.L. Sproston, G. Walker, Preliminary observations on bulk electroconvection in electrically stressed liquid insulants, Part II: theoretical Investigation, J. Electrostat. 9 (1980) 1–14.
54. T. Fujino, Y. Yokoyama, Y.H. Mori, Augmentation of laminar forced convective heat transfer by the application of a transverse electric field, ASME J. Heat Transfer 111 (1989) 345–351.
55. P.H.G. Allen, T.G. Karayiannis, Review paper: electrohydrodynamic enhancement of heat transfer and fluid flow, Heat Recovery Syst. CHP 15 (1995) 389–423.
56. J. Seyed-Yagoobi, J.E. Bryan, Enhancement of heat transfer and mass transport in single-phase and two-phase flows with electrohydrodynamics, Adv. Heat Transfer 33 (1999) 95–186.
57. S. Laohalertdecha, P. Naphon, S. Wongwises, A review of electrohydrodynamic enhancement of heat transfer, Renew. Sustain. Energy Rev. 11 (5) (2007) 858– 876.
58. A. Yabe, T. Taketani, H. Maki, K. Takahashi, Y. Nakadai, Experimental study of electrohydrodynamically (EHD) enhanced evaporator for non-azeotropic mixtures, ASHRAE Trans. 98 (2) (1992) 455–461.
59. A. Singh, M.M. Ohadi, S. Dessiatoun, M. Salehi, W. Chu, In-tube boiling enhancement of R-134a utilizing the electric field effect, in: 4th ASME/JSME Thermal Eng. Joint Conf., vol. 2, 1995, pp. 215–223.
60. M. Salehi, M.M. Ohadi, S. Dessiatoun, The applicability of the EHD technique for convective boiling of refrigerant blends-experiments with R-404A, ASHRAE Trans. 102 (1) (1996) 839–844.
61. J.E. Bryan, J. Seyed-Yagoobi, Influence of flow regime, heat flux, and mass flux on electrohydrodynamically enhanced convective boiling, J. Heat Transfer 123 (2) (2001) 355–367.
62. J. Berghmans, Prediction of the effect of electric fields on the most unstable wavelength during film boiling on small wires, J. Electrostat. (1978) 5 265– 272.
63. T.B. Jones, K.R. Hallock, Surface wave model of EHD coupled minimum film boiling, J. Electrostat. 5 (1978) 273–284.
64. A. Laures, R. Tobazéon, Electro-optical studies of liquid gaps bridged by insulating spacers, in: IEEE Conference Publication No. 129, Dielectric Materials, Measurement and Application, 1975, pp. 314.
65. H. Sadek, A.J. Robinson, J.S. Cotton, C.Y. Ching, M. Shoukri, Electrohydrodynamic enhancement of in-tube convective condensation heat transfer, Int. J. Heat Mass Transfer 49 (9–10) (2006) 1647–1657.
66. J.S. Cotton, Electrohydrodynamic condensation heat transfer modulation under dc and ac applied voltages in a horizontal annular channel, IEEE Trans. Dielectr. Electr. Insul. (2009) 495–503 (EHD special issue).
67. H. Sadek, J.S. Cotton, C.Y. Ching, M. Shoukri, In-tube convective condensation

under AC high voltage electric fields, in: 13th Int. Heat Transfer Conference (IHTC-13), Sydney, Australia, August, 2006, pp. 190–199.
68. I.W. McAllister, The dielectric strength of 1,1,1,2-C2 H2 F4 (Arcton-134a), J. Phys. D Appl. Phys. 22 (1989) 1783–1784 (Letter to the Editor).
69. B.R. Fellows, R.G. Richard, R.G., I.R. Shankland, Electrical characterization of alternative refrigerants, in: XVIIth Int. Cong. of Refrig., no. 45, Montreal Convention Center, Montreal, Quebec, Canada, 1991, pp. 398–402.
70. C. Meurer, G. Pietsch, M. Haacke, Electrical properties of CFC- and HCFCsubstitutes, Int. J. Refrig 24 (2001) 171–175.
71. T. Barao, U.V. Mardolcar, C.A. Nieto de Castro, The dielectric constant of liquid HFC 134a and HCFC 142b, Int. J. Thermophys. 17 (3) (1996) 573–585.
72. A. Sekiya, S. Misaki, The potential of hydrofluoroethers to replace CFCs and HCFCs and PFCs, J. Fluorine Chem. 101 (2001) 215–221.
73. M. Spatz, B. Minor, HFO-1234yf low GWP refrigerant: a global sustainable solution for mobile air conditioning, in: SAE 2008 Alternative Refrigerant Systems Symposium, Presentation Material, June 10–12, Scottsdale, Arizona, US, 2008.
74. R.G. Richard, Private Communication, June 14, 2000.
75. M. Spatz, B. Minor, HFO-1234yf low GWP refrigerant: a global sustainable solution for mobile air conditioning, in: SAE 2008 Alternative Refrigerant Symposium, Presentation, June 10–12, 2008 Scottsdale, AZ, 2008, pp. 1–26.
76. A.N. Gurova, T. Barao, C.A. Nieto de Castro, U.V. Mardolcar, The thermal conductivity and dielectric constant of HCFC-141b, HCFC-123, HCFC-142b, and HFC-134a, High Temp.-High Pres. 26 (1994) 25–34.
77. S.J. Kline, F.A. McClintock, Describing uncertainties in single sample experiments, Mech. Eng. (1953) 3–8.
78. J.R. Melcher, Continuum Electromechanics, The MIT Press, Cambridge, MA, USA, 1981.
79. J.S. Cotton, M. Shoukri, J.S. Chang, Oscillatory entrained droplet EHD two-phase flow, J. Heat Transfer 123 (8) (2001) 622. 7
80. H. Park, K. Kim, S. Kim, Effects of a guard plate on the characteristics of an electrospray in the cone-jet mode, J. Aerosol Sci. 35 (2004) 1295–1312.
81. Z. Liu, C. Herman, J. Kim, Heat transfer and bubble detachment in subcooled pool boiling from a downward-facing microheater array in a nonuniform electric field, Ann. N. Y. Acad. Sci. 1161 (2009) 182–191.
82. S. Siedel, S. Cioulachtjian, A.J. Robinson, J. Bonjour, Electric field effects during nucleate boiling from an artificial nucleation site, Exp. Therm. Fluid Sci. 35 (5) (2011) 762–771.
83. Tong, W., Bergles, A.E. and Jensen, M.K., Pressure drop with highly subcooled flow boiling in small-diameter tubes, *Experimental Thermal and Fluid Science*, vol. 15, pp.202–212, 1997.
84. Huo, X., Tian, Y.S. and Karayiannis, T.G., R134a flow boiling heat transfer in small diameter tubes. *Advances in Compact Heat Exchangers*, R. T. Edwards, Inc., pp.95 - 111, 2007.
85. Revellin, R. and Thome, J. R., Adiabatic two-phase frictional pressure drops in microchannels. *Experimental Thermal Fluid Science*, vol. 31, no.7, pp.673-685, 2007.
86. Coleman, J.W. and Garimella, S., Characterization of two-phase flow patterns in small diameter round and rectangular tubes. *International Journal of Heat and Mass Transfer*, vol. 42, pp.2869-2881, 1999.
87. Zhao, T.S. and Bi, Q.C., Co-current air-water two-phase flow patterns in vertical triangular microchannels, *International Journal of Multiphase Flow*, vol. 27, pp.765-782, 2001.
88. Chen, L., Tian, Y.S. and Karayiannis, T.G., The effect of tube diameter on vertical two-phase flow regimes in small tubes. *International Journal Heat Mass Transfer*, vol. 49, pp. 4220-4230, 2006.
89. Kawahara, A., Chung, P.M-Y. and Kawaji, M, Investigation of two-phase flow patterns, void fraction and pressure drop in a micro-channel. *International Journal Multiphase Flow*, vol. 28, no.9, pp.1411–1435, 2002.
90. Garimella, S. Condensation flow mechanisms in micro-channels: Basis for pressure drop and heat transfer models.

Heat Transfer Engineering, vol. 25, no.3, pp.104 – 116, 2004.

91. Thome, J.R., Dupont, V. and Jacobi, A.M., Heat transfer model for evaporation in microchannels, Part I: presentation of the model. *International Journal Heat Mass Transfer*, vol. 47, pp.3375-3385, 2004.
92. Moriyama, K., and Inoue, A., Thickness of the liquid film formed by a growing bubble in a narrow gap between two horizontal plates. *Journal Heat Transfer*, vol. 118, pp.132-139, 1996.
93. Dupont, V., Thome, J.R., and Jacobi, A.M., Heat transfer model for evaporation in microchannels, Part II: comparison with the database, *International Journal Heat Mass Transfer*, vol. 47, pp.3387-3401, 2004.
94. Shiferaw, D., Huo, X., Karayiannis, T.G. and Kenning, D.B.R., Examination of heat transfer correlations and a model for flow boiling of R134a in small diameter tubes, *International Journal Heat Mass Transfer*, vol. 50, pp.5177-5193, 2007.
95. Wen, D.S. and Kenning, D.B.R., Two phase pressure drop of water during flow boiling in a vertical narrow channel. *Experimental thermal and Fluid science*, vol. 28, no. (2-3), pp.131 – 138, 2004.
96. Shiferaw, D., Mahmoud, M.M., Karayiannis, T.G. and Kenning, D.B.R., Experimental flow boiling study in a 0.52 mm diameter vertical tube using R134a, *5th European Thermal-Sciences Conference* , Eindhoven, 18-22 May 2008.
97. Karayiannis, T.G., Shiferaw, D., Kenning, D.B.R. and Wadekar, V.V., Flow patterns and heat transfer in small to micro diameter tubes, *Heat Transfer Engineering*, vol. 31, no.4, pp. 257-275, 2010.
98. Damianides, C.A. and Westwater, J.W., Two-phase flow patterns in a compact heat exchanger and in small tubes. In *Second UK National Conference on Heat Transfer*, vol. 11, pp.1257-1268, 1988.